Volume 3
Number 10
October 2023
Pages 1377–1578

Environmental Science
Atmospheres

rsc.li/esatmospheres

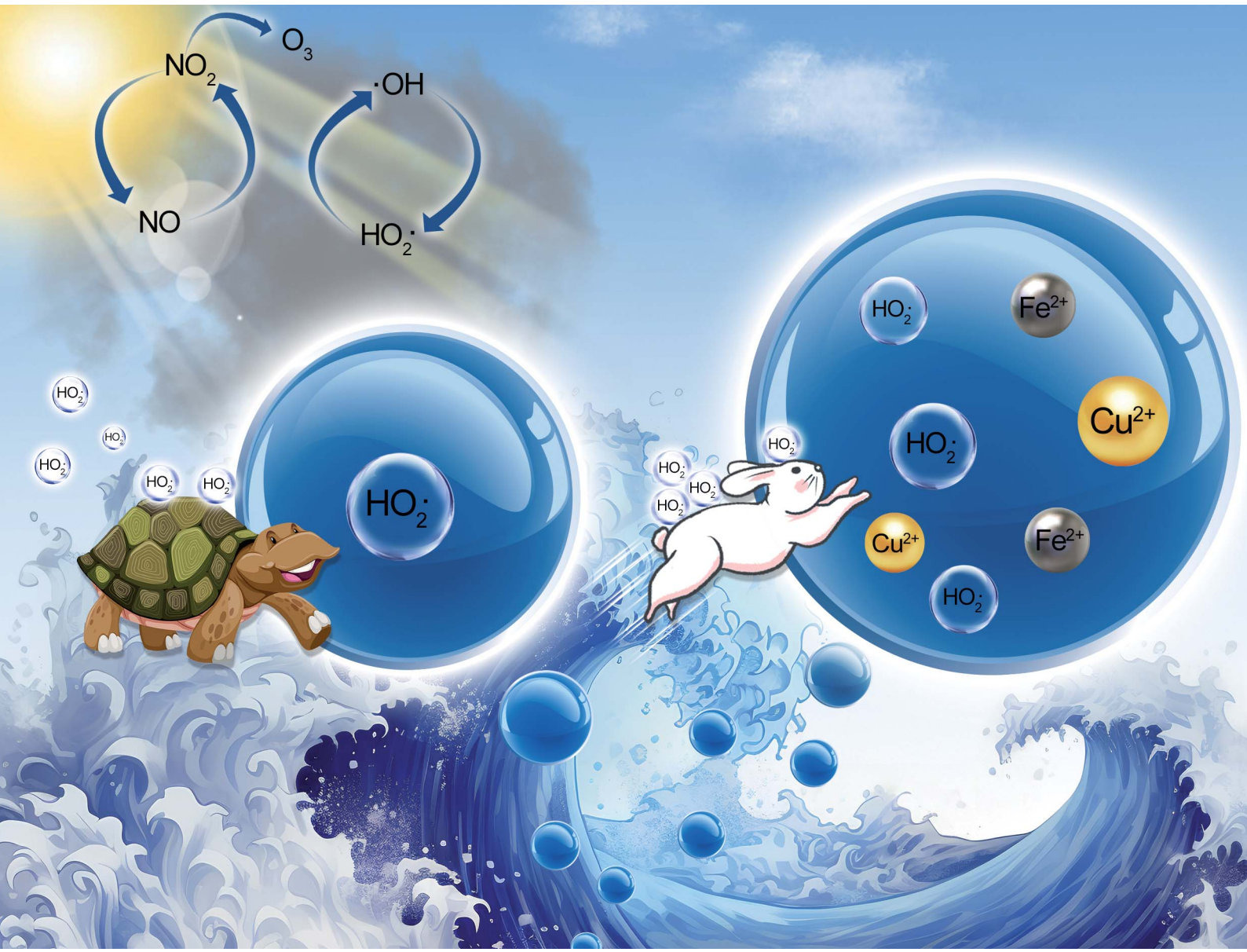

ISSN 2634-3606

ROYAL SOCIETY OF CHEMISTRY

PAPER

Yosuke Sakamoto, Yoshizumi Kajii *et al.*

Investigation of HO_2 uptake onto Cu(II)- and Fe(II)-doped aqueous inorganic aerosols and seawater aerosols using laser spectroscopic techniques

Environmental Science: Atmospheres

ROYAL SOCIETY OF CHEMISTRY

PAPER

View Article Online
View Journal | View Issue

Check for updates

Cite this: *Environ. Sci.: Atmos.*, 2023, **3**, 1384

Investigation of HO_2 uptake onto Cu(II)- and Fe(II)-doped aqueous inorganic aerosols and seawater aerosols using laser spectroscopic techniques†

Jiaru Li, [ab] Yosuke Sakamoto, *[abc] Kei Sato, [b] Yu Morino [b] and Yoshizumi Kajii *[abcd]

Heterogeneous HO_2 uptake onto aerosols, which affects tropospheric chemistry, is known as a potential sink of HO_x (≡OH + HO_2+RO_2); however, the associated reaction kinetics are still unclear. Also, the measurement of the HO_2 uptake coefficient (γ) remains challenging and the γ values reported so far based on laboratory studies vary by orders of magnitude depending on the aerosol properties, initial HO_2 concentration, and the experimental conditions. Here, we established a novel approach for detecting the loss rate of HO_2 uptake by inorganic aerosols derived from NaCl, $(NH_4)_2SO_4$, Na_2SO_4, or diluted seawater using laser-pump and laser-induced fluorescence techniques and clarified the effects of transition metal ions (TMIs), Cu(II) and Fe(II) on the process. Our results confirmed the enhancement effects of Cu(II) and Fe(II) on the uptake process. Furthermore, soluble Cu(II) enhanced the uptake with a kinetic reaction rate coefficient two orders of magnitude higher than that of Fe(II) ions. The second order rate constants of bulk phase reactions for Cu(II)- and Fe(II)-doped $(NH_4)_2SO_4$ are 1.5×10^7 M^{-1} s^{-1} and 1.3×10^5 M^{-1} s^{-1}, respectively. However, uncertainties regarding the pH of the aerosols and TMI participation in the aerosol phase still exist. Notwithstanding, the uptake coefficients here reported will complement current IUPAC recommendations. Additionally, future studies can benefit from investigations of the effects of aerosol pH on the HO_2 uptake process, the determination of uptake onto other TMI-doped aerosol types, and testing with ambient aerosols. Our findings can also be incorporated into multiphase kinetic models for a better understanding of the bulk and surface processes and for the evaluation of spatiotemporal oxidation products under ambient atmospheric conditions.

Received 23rd June 2023
Accepted 23rd August 2023

DOI: 10.1039/d3ea00093a

rsc.li/esatmospheres

Open Access Article. Published on 24 August 2023. Downloaded on 5/25/2026 11:43:11 AM.
This article is licensed under a Creative Commons Attribution-NonCommercial 3.0 Unported Licence.

Environmental significance

HO_2 uptake by aerosols is a potential loss pathway that influences the key atmospheric radical budget and has been coarsely considered in most oxidant simulations. Understanding the multiphase reactions under which the interaction parameter is well controlled is crucial to deepen our understanding. In this work we look at how doped metal ions and parent inorganic species affect the heterogeneous HO_2 uptake. We also determined the kinetic parameters, such as the uptake coefficient, surface accommodation factor, and reactional rate in the aerosol phase of the HO_2 uptake process, which can be factored into models for the precise evaluation of the radical budget in the atmosphere to help bridge the gap between model results and field observations.

1 Introduction

The uptake of hydroperoxyl (HO_2) radicals by aerosols potentially affects volatile organic compound (VOC) oxidation, ozone formation, and secondary organic aerosol generation, given that HO_2 is a major OH reservoir under atmospherically relevant conditions.[1–3] Additionally, the uptake process can impact the climate by altering aerosol properties, such as size, optical properties, and nucleation.[4] However, the multiphase reaction pathways involved in the uptake process, which are important for both atmospheric chemistry and climate modelling, are not yet well understood. In essence, the uptake process of HO_2 competes with gas-phase reactions and may significantly change the chemical composition of air. For example, aerosol uptake has been shown to be responsible for up to 23% of HO_2 loss based on modelled and measured HO_2 concentrations in the tropical marine area at noon.[5] Some research groups recommended the use of an uptake coefficient (γ) of 0.2 for the estimation of HO_2 uptake onto aerosols.[6–9] Furthermore, an

[a]*Graduate School of Global Environmental Studies, Kyoto University, Kyoto, 606-8501, Japan. E-mail: sakamoto.yosuke.7a@kyoto-u.ac.jp; kajii.yoshizumi.7e@kyoto-u.ac.jp*
[b]*National Institute for Environmental Studies, Tsukuba, 305-8506, Japan*
[c]*Graduate School of Human and Environmental Studies, Kyoto University, Kyoto, 606-8316, Japan*
[d]*School of Environmental Science and Engineering, Qingdao University, Qingdao, 266071, P. R. China*

† Electronic supplementary information (ESI) available. See DOI: https://doi.org/10.1039/d3ea00093a

© 2023 The Author(s). Published by the Royal Society of Chemistry

Open Access Article. Published on 24 August 2023. Downloaded on 5/25/2026 11:43:11 AM.
This article is licensed under a Creative Commons Attribution-NonCommercial 3.0 Unported Licence.

empirical model known as the MARK model depicts the uptake of HO_2 onto wet aerosols and has been applied in field campaigns. However, the results obtained by MARK showed large variations considering HO_2 uptake onto Cu-doped aerosols.[10] Consequently, aerosol-inhabited photochemical ozone production reached a ratio as high as 18–35% in the 1970s in Japan, Europe, and America, and 20–35% in 2014 in China.[8]

Aerosols consist of a diverse range of chemical components and usually exist under aerodynamic conditions. Thus, investigating the multiphase reactions of radicals with aerosols is challenging. Soluble transition metal ions (TMIs), such as iron(II) and copper(II) ions, are hazardous components of fine particles and are associated with adverse health effects. Previous studies have linked the increased oxidative potential of atmospheric particles to the presence of soluble TMIs.[11,12] Copper and iron were selected for this study owing to their abundance in the atmospheric environments, including combustion and dust aerosols, their active reactivities, and because they are the most widely investigated transition metals.[13,14] However, the kinetic roles of TMIs such as Cu(II) and Fe(II) in heterogeneous reactions are not well understood. Table 1 summarizes the uptake coefficients of HO_2 radicals onto NaCl, $(NH_4)_2SO_4$, and Cu(II)-doped aerosols and seawater based on previous studies. Currently, studies on the heterogeneous radical loss rate are limited, and in most previous studies we compared, an aerosol flow-tube (AFT) reactor was combined with a laser-induced fluorescence detector or a chemical ion mass spectrometer to investigate the heterogeneous radical loss rate. The first measurement of HO_2 uptake by aqueous aerosols was realized using an AFT reactor combined with a peroxyl radical chemical amplification-luminol detector under humid conditions.[15] The AFT controls the residence time of the radicals by varying the injection points and detects the corresponding radical concentrations after they interact with aerosols. However, such an approach requires manual control of radical injection, and this results in a low time resolution. Furthermore, extra calibration work is necessary to determine the initial HO_2 concentration, although it depends on the detection techniques. Considering that the uptake coefficient varies with the initial radical concentration, aerosol chemical and physical properties, and experimental conditions, such as temperature and relative humidity (RH), an effective approach that enhances understanding regarding multiphase reactions in this regard is necessary.

The current study combines the chemical conversion (CC) method with a laser-pump and laser-induced fluorescence (LP-LIF) to determine the loss rate of HO_2 radicals onto aerosols as a depiction of OH reactivity (the inverse of the OH lifetime) by converting HO_2 into OH before detection. Deliquesced aerosols, including (i) NaCl, (ii) $(NH_4)_2SO_4$, (iii) Na_2SO_4, and (iv) seawater, were generated using a commercial constant-output atomizer, and TMIs such as Cu(II) or Fe(II) were added to the dissolved reagent to examine their doping effects. The CC/LP-LIF offered the possibility to detect the loss rate of HO_2 radicals by controlling the sampling of air, either with or without aerosols, to separate heterogeneous HO_2 loss from gas-phase loss. Also, it is flexible to detect the HO_2 loss rate onto varied total aerosol surface area concentrations by changing the flow rate of zero-gas passing through the atomizer. Note that the residence time of HO_2 mixing with aerosols in the reaction cell is short at 1 s, allowing high time resolutions and there is no need to change the interaction time using our apparatus. The AFT-reactor approach requires a movable injector to change the reaction time of radicals with aerosols, and detect different radical concentrations at varied time to determine its loss rate. However, we directly measure the loss rate of radicals with increased/decreased volume of aerosols to obtain their uptake coefficient. Furthermore, no additional calibration was required because we measured HO_2 reactivity rather than its concentration. It is also possible to detect RO_2 uptake using our method. Thus, we established a novel measurement strategy for determining HO_2 uptake by applying the CC/LP-LIF method with an atomizer, and this is different to the AFT-reactor approach, which requires controlling of the injection of radicals. Table 2

Table 1 Reported uptake coefficients of HOx radicals by inorganic aerosols. Only results obtained in studies conducted under the most humid experimental conditions and related to the current study are presented

Aerosol	γ	Initial $[HO_2]$ molecules cm^{-3}	RH	References
NaCl	0.01 ± 0.02	$\sim 1.5 \times 10^9$	67–76%	George *et al.* (2013)[42]
	0.10 ± 0.02	$\sim 1 \times 10^8$	75%	Taketani *et al.* (2008)[43]
NaCl + Cu(II)	0.65 ± 0.17	$\sim 1 \times 10^8$	53%	Taketani *et al.* (2008)[43]
$(NH_4)_2SO_4$	$\sim 0.1^a$	$2.5–5 \times 10^{10}$	42%	Thornton and Abbatt (2005)[36]
	0.01 ± 0.01	$\sim 1.5 \times 10^9$	65–75%	George *et al.* (2013)[42]
	0.19 ± 0.04	$\sim 1 \times 10^8$	75%	Taketani *et al.* (2008)[43]
	0.004 ± 0.002	$\sim 1 \times 10^9$	60%	Lakey *et al.* (2016b)[27]
	0.001 ± 0.0007	$\sim 1 \times 10^9$	51%	Zou *et al.* (2019)[44]
$(NH_4)_2SO_4$ + Cu(II)	0.5 ± 0.1	$2.5–5 \times 10^{10}$	42%	Thornton and Abbatt (2005)[36]
	0.4 ± 0.3	$\sim 1.5 \times 10^9$	53–65%	George *et al.* (2013)[42]
	0.53 ± 0.13	$\sim 1 \times 10^8$	45%	Taketani *et al.* (2008)[43]
	0.23 ± 0.07	$\sim 1 \times 10^9$	60%	Lakey *et al.* (2015)[32]
Synthetic sea salt	0.13 ± 0.04	$\sim 1 \times 10^8$	75%	Taketani *et al.* (2009)[33]
Natural seawater	0.10 ± 0.02	$\sim 1 \times 10^8$	75%	Taketani *et al.* (2009)[33]

[a] Experiment conducted using $(NH_4)_2SO_4$ buffered to pH 5.1.

Open Access Article. Published on 24 August 2023. Downloaded on 5/25/2026 11:43:11 AM.
This article is licensed under a Creative Commons Attribution-NonCommercial 3.0 Unported Licence.

Table 2 Comparison of the AFT-reactor approach from the Leeds group and the apparatus used in the current work

		AFT-reactor[45]	LP-LIF/CC
HO_2 generation		Photolysis of water vapor	Pump-flush of ozone
Mixing time required		7 s	—
Residence time of radicals		7–20 s (depending on the injector place and flow rate)	1 s
Buffer gas		N_2	Zero-gas
Reaction cell conditions	Temperature	−10 to 40 °C, mostly room temperature	Room temperature
	Pressure	Atmospheric pressure	Atmospheric pressure
	RH	5–80%	>80%
Detection objective		HO_2 concentration	HO_2 reactivity
Time resolution		In the unit of 10 min	4 min
Calibration		Concentration calibration and wall loss correction	Blank measurement
Further application			Easy to change to detect RO_2 uptake

compares the details between the AFT-reactor and our apparatus. We also compared the determined uptake coefficient with previously reported values to demonstrate the credibility of our method. We further examined its sensitivity to impacting factors, such as parent aerosols, TMI doping, and potential kinetic parameters including pH which affect the rate constant in the aerosol phase. These results are advantageous for studying heterogeneous processes and evaluating the oxidative potential of typical particulate matter.

2 Experimental

2.1 CC/LP-LIF

The reactivity of HO_2 radicals was investigated *via* LP-LIF[16] using the CC method.[17] In brief, sampled air was pumped into an aluminum reaction cell (length and i.d. of 1.4 m and 40 mm, respectively) at a total flow rate of ∼14 SLM (standard litter per minute under conditions of 1 atm and 273 K). A pulsed beam was pumped from a fourth harmonic Nd:YAG laser (Tempest 300, 5.5 mJ per pulse, New Wave Research Inc., Fremont, CA, USA) with a wavelength of 266 nm to photolyze ∼80 ppbv of ozone in the sample so as to generate OH radicals, as shown in (R1) and (R2). The ozone used was generated using a low-pressure mercury lamp irradiated at 184.9 nm. Water vapor was obtained from the air flow passing through a bubbler containing ultrapure water (18.2 MΩ cm and 2.4 ppb TOC at 25 °C, Milli-Q, Millipore Corp., Bedford, MA, USA). The initial concentration of radicals was in the order of 10^{10} molecules cm^{-3} based on the maximal photolysis laser power and ozone concentration and could vary with RH. In our later discussion, the initial radical concentration was assumed to be 1×10^{10} molecules per cm with an uncertainty of −50%. HO_2 radicals were produced in the reaction cell *via* the excess addition of CO, as shown in (R3). Under all conditions, the self-reaction of HO_2 in the gaseous and aqueous phases could be excluded from the zero-gas measurements and uptake results for the ultrapure water-generated aerosols, respectively.

$$O_3 + h\nu\ (266\ nm) \rightarrow O_2 + O(^1D) \quad (R1)$$

$$O(^1D) + H_2O \rightarrow 2OH \quad (R2)$$

$$OH + CO \xrightarrow{O_2} HO_2 + CO_2 \quad (R3)$$

A portion of the gases from the reaction cell was introduced into the LIF cell through a 0.5 mm orifice at 2 SLM and ∼2 Torr using an oil rotary pump (D-950, ULVAC, Kanagawa, Japan). In the LIF cell, 10 kHz irradiation was pumped by a second-harmonic Nd:YVO_4 laser (YHP40-532Q, Spectra Physics, Mountain View, CA, USA), which then excited a second-harmonic pulsed dye laser (Credo-D, Sirah) at 308 nm. The LIF signal was detected using a photomultiplier tube (PMT, R2256P, Hamamatsu Photonics, Shizuoka, Japan) comprising four lenses and a bandpass filter centered at approximately 308 nm. For both excitation and detection, the A-X(0,0) band of OH was used, and the fluorescence from the $Q_1(2)$ line was collected *via* time filtering controlled by a delay generator (DG535, Stanford Research Systems, Sunnyvale, CA, USA) providing a positive transistor–transistor logic pulse. The detection axis was positioned vertically to both the gas flow and excitation laser, as shown in Fig. 1, to avoid any possible interference. Furthermore, the generated HO_2 radicals were reconverted into OH radicals *via* reaction with NO before introduction into the LIF cell (R4). Each decay rate was averaged every 240 cycles, which were repeated at 4 min intervals.

$$HO_2 + NO \rightarrow OH + NO_2 \quad (R4)$$

2.2 Aerosol generation and property detection

Reagents (0.03% w/v) containing 0.0015% w/v TMIs or L-ascorbate were dissolved in ultrapure water. Then, to obtain polydisperse aerosols, the mixture was passed through a pneumatic atomizer (Model 3076, TSI, St. Paul, MN, USA) at a flow rate of 1.5–2.4 SLM. The chemical materials used included NaCl (99.5%, Fujifilm Wako, Osaka, Japan), $(NH_4)_2SO_4$ (99.5%, Wako), Na_2SO_4 (99.0%, Fujifilm Wako), $CuCl_2 \cdot 2H_2O$ (99.9%, Fujifilm Wako), $FeCl_2 \cdot 4H_2O$ (99.9% Fujifilm Wako), $CuSO_4 \cdot 5H_2O$ (99.9%, Fujifilm Wako), $FeSO_4 \cdot 7H_2O$(99.5%, Fujifilm Wako), and L-ascorbate (99.6%, Nacalai Tesque, Kyoto, Japan), as listed in Table 3. Regarding the TMI-doped aerosols, the

© 2023 The Author(s). Published by the Royal Society of Chemistry

Open Access Article. Published on 24 August 2023. Downloaded on 5/25/2026 11:43:11 AM.
This article is licensed under a Creative Commons Attribution-NonCommercial 3.0 Unported Licence.

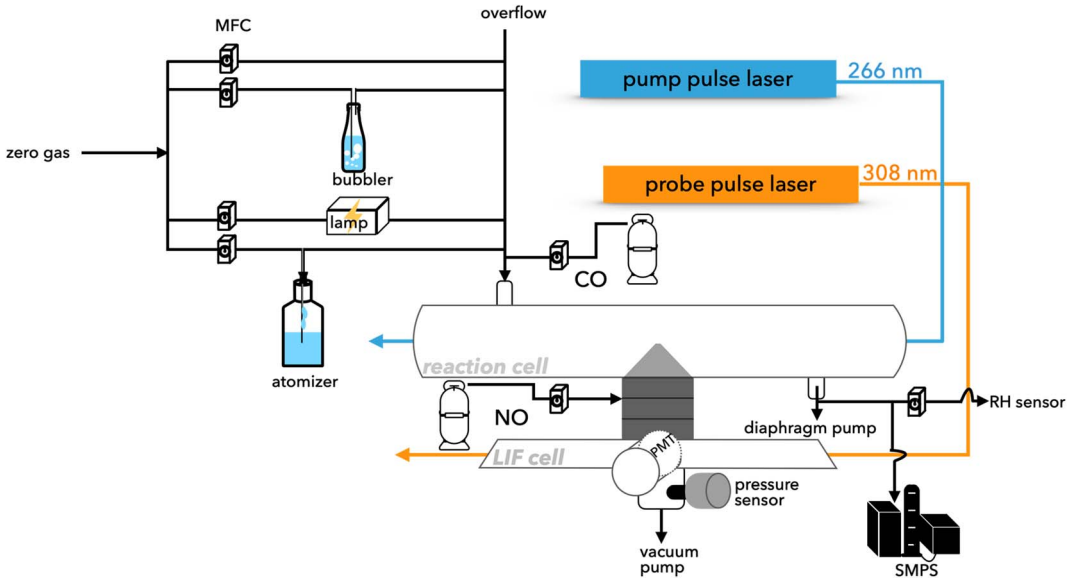

Fig. 1 Schematic of the simplified detection system.

same anion type was used to avoid potential interference. The aerosols were then introduced into the reaction cell and mixed with zero-gas that passed through a bubbler for humidity conditioning. The temperature and humidity inside the reaction cell were measured in real-time using a Vaisala HMT334 probe (Vantaa, Finland).

Seawater samples collected from two islands in Japan, Izu (34°58′N, 138°56′E) and Hachijojima (33°25′N, 139°50′E), were diluted a hundred-fold using ultrapure water and used to produce seawater aerosols containing approximately 0.03% (w/v) NaCl. The Izu sample was buffered with additives to maintain the pH at 8.3. Some of the chemical components of the sample from Hachijojima were measured, as indicated in Appendix Table A1.†

The size distribution of the aerosols in the reaction cell was detected simultaneously using a scanning mobility particle sizer (SMPS: TSI) which comprised a condensation particle counter (CPC; model 3752) and a differential mobility analyzer (DMA; Electrostatic Classifier model 3082 with a long DMA 3081A). The DMA selects a monodisperse fraction after the aerosols are charged in an electric field and then detects them using a CPC. Appendix Fig. A1† shows the distribution of

Table 3 Information regarding atomizer-generated aqueous aerosols and corresponding uptake coefficients with the 2σ value of the uncertainty

Solutions	RH	γ_{eff}	γ	References
NaCl	82.1%	0.03 ± 0.01	0.03 ± 0.01	0.01 ± 0.02[a]
				0.10 ± 0.02[b]
NaCl + Cu(II)	74.4%	0.65 ± 0.17	0.72 ± 0.17	0.65 ± 0.17[b]
NaCl + Fe(II)	83.5%	0.27 ± 0.06	0.28 ± 0.06	
NaCl + L-ascorbic acid	82.4%	0.40 ± 0.15	0.46 ± 0.15	
$(NH_4)_2SO_4$	83.7%	~0.01	~0.01	0.001 ± 0.0007[c]
				0.004 ± 0.002[d]
				0.01 ± 0.01[a]
				0.19 ± 0.04[b]
				~0.1[e]
$(NH_4)_2SO_4$ + Cu(II)	85.6%	0.60 ± 0.19	0.67 ± 0.19	0.23 ± 0.07[f]
				0.4 ± 0.3[a]
				0.53 ± 0.13[b]
				0.5 ± 0.1[e]
$(NH_4)_2SO_4$ + Fe(II)	83.3%	0.25 ± 0.05	0.26 ± 0.05	0.10 ± 0.02[g]
Na_2SO_4	83.6%	0.04 ± 0.00	0.04 ± 0.00	
Na_2SO_4 + Cu(II)	82.1%	0.49 ± 0.21	0.56 ± 0.21	
Na_2SO_4 + Fe(II)	83.3%	0.16 ± 0.02	0.17 ± 0.02	
Seawater (Izu)	82.2%	0.11 ± 0.01	0.12 ± 0.01	
Seawater (Hachijojima)	78.9%	0.22 ± 0.04	0.24 ± 0.04	

a George et al., 2013. *b* Taketani et al., 2008. *c* Zou et al. (2019). *d* Lakey et al. (2016b). *e* Thornton and Abbatt (2005). *f* Lakey et al. (2015). *g* Taketani et al. (2009).

Open Access Article. Published on 24 August 2023. Downloaded on 5/25/2026 11:43:11 AM. This article is licensed under a Creative Commons Attribution-NonCommercial 3.0 Unported Licence.

aerosol surface area density as a function of gas flow passing through the atomizer. Over the mobility diameter range (14.6–661.2 nm), all profiles could be characterized *via* lognormal radius distribution with the geometric mean diameter distributed at approximately 100–140 nm.

2.3 HO_2 uptake onto aerosols

The detected loss rate of the radicals included the zero-gas loss rate, as explained in eqn (1), which can be explored using a single exponential fitting equation, assuming pseudo-first-order reactions. Fig. A2(a)† compares the decay profiles of the radicals from zero-gas-only and zero-gas with aqueous NaCl aerosols. In the presence of aerosols, the LIF intensity decreases at a faster rate, and the discrepancy in decay rates represents the heterogeneous radical loss rate, k', which varies with the volume of the generated aerosols. The total surface area concentrations of aerosols generated by the atomizer can be varied using different flow rates as introduced in Section 2.2. Consequently, larger total surface area concentrations result in faster decay rates. Different to the AFT-reactor approach, we fixed the residence time of radicals and aerosols in the reaction cell as 1 s, and then regenerated radicals every second. The determined decay rate of HO_2 radicals was averaged every 240 cycles. Each experiment was repeated three–five times to ensure reproducibility and reduce uncertainty. Then we measured with a varied volume of aerosols to extrapolate the relationship between decay rates and total surfaced area concentrations in order to quantify the effective uptake coefficient. Before switching to a different aerosol type, ultrapure water was used to flush the atomizer and reaction cell until the decay rate from ultrapure water-generated aerosols was the same as that from zero-gas. More details regarding the uptake mechanism are discussed later.

$$\frac{\mathrm{d}[\mathrm{OH}]}{\mathrm{d}t} = -\left(k' + k_{\mathrm{zero}}'\right)[\mathrm{OH}] \tag{1}$$

The effective uptake coefficient can be calculated using eqn (2), where k' represents the heterogeneous loss rate of the radicals, extrapolated from eqn (1), ω refers to the mean molar velocity of HO_2, and S is the total surface area of the aerosol.

$$\gamma_{\mathrm{eff}} = \frac{4k'}{\omega S} \tag{2}$$

Eqn (3) shows that ω can be determined from the temperature and molar weight according to the probability distribution normalized by all the possible molar speeds. In the case of HO_2, $\omega = 43\,724.64$ cm s^{-1} was used.

$$\omega = \sqrt{\frac{8RT}{\pi M}} \tag{3}$$

The uptake process involves gas-phase diffusion effects, which decrease the concentration of radicals in the vicinity of the aerosols. Such effects of diffusion, Γ_g, could be excluded as shown in eqn (4).

$$\frac{1}{\gamma_{\mathrm{eff}}} = \frac{1}{\Gamma_g} + \frac{1}{\gamma} \tag{4}$$

Gas phase diffusion effects depend on the Knudsen number, which is determined as the gas phase mean free path (λ) to particle radius (r) ratio as shown in eqn (5) and (6). Specifically, λ gives the average distance travelled by a radical before collision with particles, and can be determined using the gas phase diffusion coefficient of HO_2 (D_g) and ω. Reportedly, the value of D_g is 0.25 cm^2 s^{-1} at room temperature and 760 Torr.[15]

$$\frac{1}{\Gamma_g} = \frac{0.75 + 0.28K_n}{K_n(1 + K_n)} \tag{5}$$

$$K_n = \frac{3D_g}{\omega r} = \frac{\lambda}{r} \tag{6}$$

Similar K_n values have been reported for inorganic and organic compounds, regardless of their varied diffusivities, and this has been attributed to their similar mean free paths in air under a given pressure.[18] In this study, the exclusion of gas diffusion effects could bring about an increase in γ by up to 11% depending on the initial γ_{eff} and particle radius.

2.4 Investigation of γ using a resistance model

(R5) and (R6) show the chemical reactions of heterogeneous HO_2 uptake, which depends on the mass accommodation coefficient (α) and bulk phase reactions (Γ_p), as shown in eqn (7).

$$\mathrm{HO_2(g)} \rightarrow \mathrm{H^+(aq)} + \mathrm{O_2^-(aq)} \tag{R5}$$

$$\mathrm{HO_2(g)} \rightarrow \mathrm{HO_2(aq)} \tag{R6}$$

$$\frac{1}{\gamma} = \frac{1}{\alpha} + \frac{1}{\Gamma_p} \tag{7}$$

Γ_p in eqn (7) is related to the self-reaction of HO_2/O_2^- in the aqueous phase, as shown in (R7) and (R8).

$$\mathrm{HO_2(aq)} + \mathrm{HO_2(aq)} \rightarrow \mathrm{H_2O_2(aq)} + \mathrm{O_2(aq)} \tag{R7}$$

$$\mathrm{HO_2(g)} + \mathrm{O_2^-(aq)} + \mathrm{H_2O} \rightarrow \mathrm{H_2O_2(aq)} + \mathrm{O_2(aq)} + \mathrm{OH^-(aq)} \tag{R8}$$

Furthermore, Γ_p, which can be calculated according to eqn (8),[19] strongly depends on the gas phase concentration of HO_2. It also determines $[HO_2]_{aq}$ and $[O_2^-]_{aq}$ and quadratically causes the loss of aqueous phase HO_2. k_{aq} is the second-order rate constant of HO_2/O_2^- and varies with pH in the aqueous phase (see eqn (9)),[20] and K_{eq} represents the equilibrium constant, which at 298 K, is 2.1×10^{-5} M.[6] k_7 (8.3×10^5 M^{-1} s^{-1}[20]) and k_8 (9.7×10^7 M^{-1} s^{-1}[20]) are the rate constants for (R7) and (R8), respectively, while H represents henry's constant, which is explained later.

$$\Gamma_p = \frac{8000(HRT)^2 k_{aq}[HO_2]r_p}{3\omega N_{Av}} \tag{8}$$

© 2023 The Author(s). Published by the Royal Society of Chemistry

Open Access Article. Published on 24 August 2023. Downloaded on 5/25/2026 11:43:11 AM.
This article is licensed under a Creative Commons Attribution-NonCommercial 3.0 Unported Licence.

$$k_{aq} = \frac{k_7 + \left(K_{eq}/[H^+]_{aq}\right)k_8}{\left(1 + K_{eq}/[H^+]_{aq}\right)^2} \quad (9)$$

In the presence of TMIs, the loss process of HO_2 or O_2^- might be dominated by bulk phase reactions with TMIs (Γ_{TMI}), which occur much faster than self-reactions. Thus, eqn (7) can be written as eqn (10) when the slow self-reactions of HO_2/O_2^- (Γ_p) are replaced by the sum of Γ_{TMI} and Γ_p. The α value used was 0.7, the maximal determined uptake coefficient (Table 3).

$$\frac{1}{\gamma} = \frac{1}{\alpha} + \frac{1}{\Gamma_{TMI} + \Gamma_p} \quad (10)$$

In the case of the TMIs involved in the aqueous phase, the loss process may be given by eqn (11),[21] which includes the correction of saturation, assuming that uptake occurs on spherical particles of radius r_p. Specifically, r_p can be estimated from the detected total surface area and the total number of aerosols, according to eqn (12). l_{rd} is the reacto-diffusion length, as expressed in eqn (13).

$$\frac{1}{\Gamma_{TMI}} = \frac{\omega}{4HRT\sqrt{D_{aq}k_{TMI}[TMI]}\left[\coth\left(\frac{r_p}{l_{rd}}\right) - \left(\frac{l_{rd}}{r_p}\right)\right]} \quad (11)$$

$$r_p = \sqrt{\frac{S}{4\pi N}} \quad (12)$$

$$l_{rd} = \sqrt{\frac{D_{aq}}{k_{TMI}[TMI]}} \quad (13)$$

In eqn (14), H represents henry's constant for HO_2. The effects of aerosol pH and HO_2 activity are discussed in Section 3.3. Furthermore, D_{aq} in eqn (15) represents the aqueous-phase diffusive constant, which was approximated based on $(NH_4)_2SO_4$ solutions as reported by IUPAC.[22] In the present study, only inorganic solutes were considered; thus, there were no significant differences in viscosity, *i.e.*, the same D_{aq} was used for all the other inorganic solutes as was used for $(NH_4)_2SO_4$.

$$H = 9.5 \times 10^{-6}\exp\left(\frac{5910}{T}\right)\left(1 + \frac{K_{eq}}{[H^+]}\right) \text{ M per atm} \quad (14)$$

$$D_{aq} = \left\{1 \times 10^{-5}\left(\frac{T}{298}\right)\right\} \Big/ \left(1.09 \times 10^8 \exp(-0.068T) + 0.873\right) \quad (15)$$

2.5 Model simulations

The concentrations of TMIs in the aerosol phase estimated from the thermodynamic equilibrium modelling of E-AIM[23,24] and ISORROPIA[25,26] are compared as shown in Table A2.† We assessed the TMI concentrations indirectly by assuming the same change of the ratio as the water content in the aerosol phase compared to the liquid phase. A same change ratio of the condensed TMIs was assumed to simulate the concentrations in the aerosol phase. Given that the two models agreed well with each other in most cases, we used the E-AIM-based results in the subsequent calculations. It is also worth noting that TMI concentrations from E-AIM do not consider the activity coefficients of ions; thus, there may be uncertainties regarding the activity of the TMIs in the bulk phase reaction. Aerosol pH was also simulated by using thermodynamic models, and the details will be available in Section 3.3.

3 Results and discussion

3.1 Instrument performance and detection limit

CC/LP-LIF was successfully used to detect the loss rate of HO_2 onto deliquesced aerosols. Fig. 2 shows the decay rate of the heterogeneous HO_2 loss rate, k', with respect to the varied surface area concentrations of the aerosols. From this figure, it is evident that k' increased linearly with increasing aerosol surface area concentration, and from the slope of each line, the effective uptake coefficient was calculated using eqn (2). In the case of $(NH_4)_2SO_4$, the average HO_2 uptake coefficient was ~0.01, consistent with the value previously reported by Lakey *et al.* ($\gamma = 0.004 \pm 0.002$)[27] and George *et al.* ($\gamma = 0.01 \pm 0.01$).[28] Generally, the results of this study showed good reproducibility and the extrapolated γ agreed well (within uncertainty) with most reported values obtained in studies conducted under similar experimental conditions as summarize in Table 1. However, there should be discrepancies between our results and other reported γ owing to different experimental conditions such as aerosol water content, radical concentration, interaction time of radicals and aerosols, and different hypothesized parameters used to quantify the γ. More discussion in depth will be described in Section 3.2 to indicate the difference of our result compared with previous results.

The detection limit (LOD) of γ based on the LP-LIF technique was estimated based on the lower limit of the measurement, with the daily zero-gas uncertainty of HO_2 reactivity determined to be ~0.1 s^{-1} (mostly under RH >75%). The lower limit of the uptake coefficient may also depend on the total aerosol surface area concentration, as shown in Fig. A2(b).† In essence, the maximal concentration of the total aerosol surface area produced from an atomizer is 7.5×10^{10} in the unit of nm^2 cm^{-3}, and this allows the detection of γ values larger than 0.01. Note that the total aerosol surface area concentration generated in the reaction cell strongly depends on RH, *i.e.*, the water content of aerosols, which is determined by the dilution rate of wet zero-gas. Therefore, with lower RH the LOD should be larger. In addition, given that the γ from $(NH_4)_2SO_4$ aerosols is close to the LOD, we did not report its uncertainty.

3.2 Uptake coefficients of HO_2 onto deliquesced inorganic aerosols

The comparison of the uptake coefficients of the different inorganic aerosols used in the present study is shown in Table 3

Open Access Article. Published on 24 August 2023. Downloaded on 5/25/2026 11:43:11 AM.
This article is licensed under a Creative Commons Attribution-NonCommercial 3.0 Unported Licence.

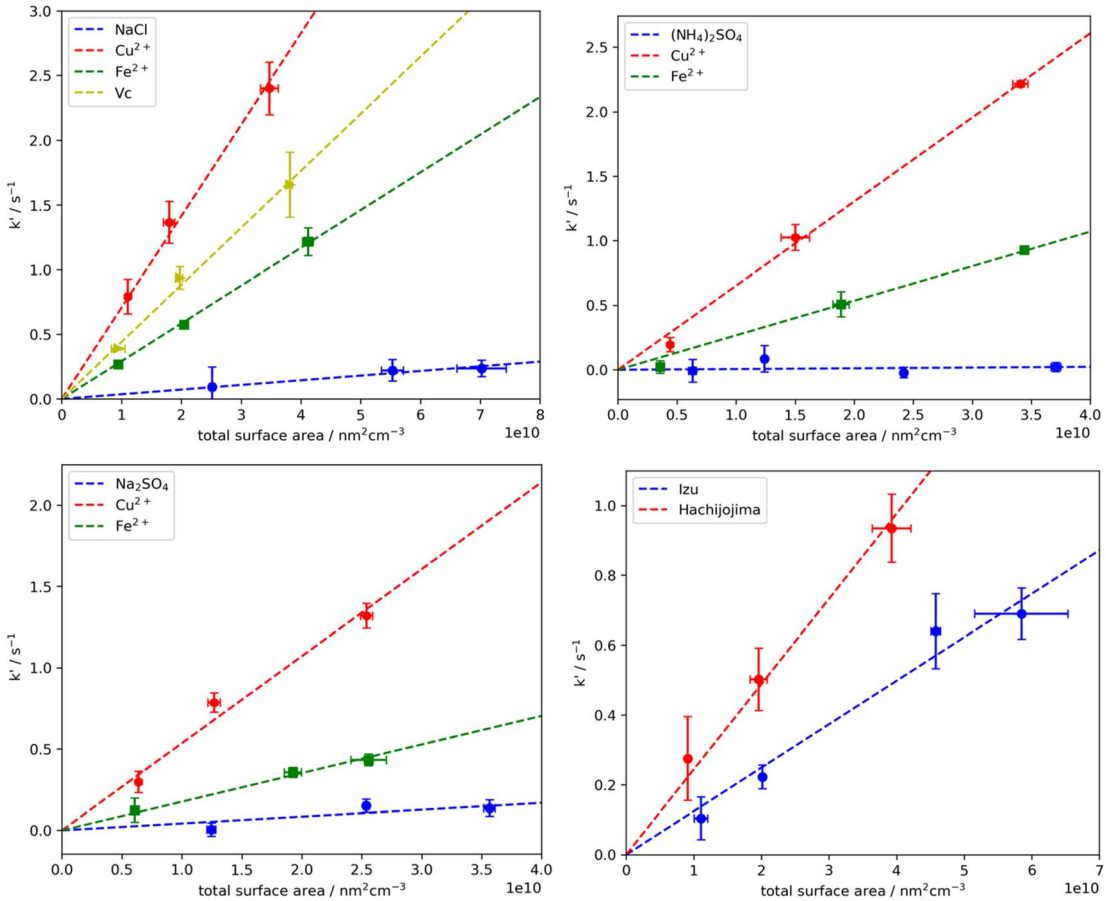

Fig. 2 Detected loss rate of HO_2 radicals from a variety of inorganic deliquescent aerosols *versus* total surface area concentration. The marker is the detected result and the error bar is based on 2σ standard deviation. The dashed lines are fitting results.

and Fig. 3. For experiments with NaCl aerosols, L-ascorbate was further dissolved in the aqueous phase for the determination of γ. As a redox active component, L-ascorbate acts as an effective HO_2/O_2^- scavenger.[29] Fig. 2 and 3 exhibit the loss rates and corresponding uptake coefficients obtained in this study under all conditions. Based on the comparison shown in Table 3, the γ values from NaCl, $(NH_4)_2SO_4$, Cu(II)-doped $(NH_4)_2SO_4$, and seawater aerosols were consistent with previously reported γ values obtained under similar high RH conditions. To date, there have been no experimental data regarding HO_2 uptake onto Fe(II)-doped inorganic aerosols. However, box models have been used to simulate HO_2 uptake in systems involving the coupling of Cu(I)/Cu(II) and Fe(II)/Fe(III) for the production of H_2O in aqueous aerosols and for a sustained level of Fe(II) driven by Cu–Fe redox coupling.[30,31] In this study, we report the largest γ value that has been obtained to date from Cu(II)-doped NaCl aerosols (0.72 ± 0.17). This value was used for a presumed α value of 0.7 in the later discussion, providing the upper limit of the detected γ value when the mass accommodation becomes identical to the evaporation coefficient in a state of equilibrium. All the synthesized aerosols showed an increase in the γ value in the presence of Cu(II) and Fe(II). L-ascorbate accelerated the uptake process faster than Fe(II), but slower than Cu(II). Previously reported HO_2 uptake coefficients onto organic aerosols also confirmed the enhancement effects of Cu(II) and Fe(II) as HO_2 scavengers at room temperature and ambient pressure.[32] For the first time, the uptake coefficients of seawater spray from

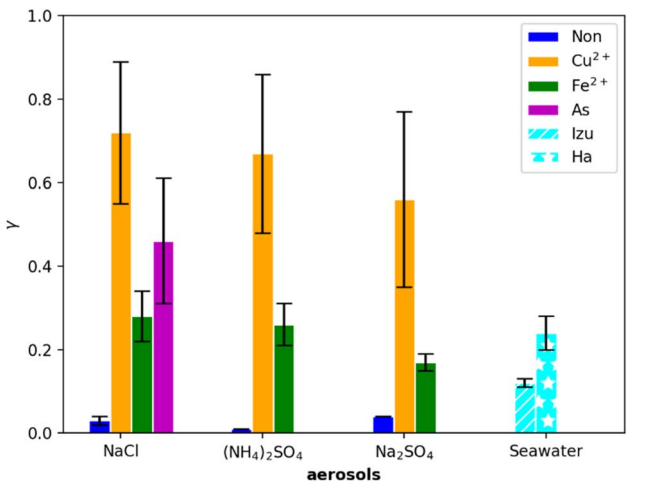

Fig. 3 Uptake coefficient, γ, with respect to the group of generated aerosols. The blue, orange, green, and magenta bars represent results corresponding to no-TMIs, Cu(II)-doped, Fe(II)-doped, and L-ascorbate-added aerosols. The results of seawater from Izu and Hachijojima are located at the extreme right.

© 2023 The Author(s). Published by the Royal Society of Chemistry

Open Access Article. Published on 24 August 2023. Downloaded on 5/25/2026 11:43:11 AM.
This article is licensed under a Creative Commons Attribution-NonCommercial 3.0 Unported Licence.

two different sampling sites were compared. We observed that the results varied from 0.12 ± 0.01 (Izu) to 0.24 ± 0.04 (Hachijojima). Taketani *et al.*[33] reported a γ value similar to that obtained for the Izu sample based on their experiment involving diluted natural seawater from Rishiri island. Seawater is a complicated mixture of a variety of dissolved inorganic components which also including TMIs. The increased salinity of seawater could be attributed to the large ionic strength of seawater, which inhibited the uptake process. In addition, ionic strength varies naturally across aquatic ecosystems. The salinity is 35.16504 g kg^{-1} for standard seawater[34] and the ionic strength is <1 M. Both Izu and Rishiri are located close to the mainland; thus, they may be characterized by a high level of biodiversity within the seawater owing to anthropogenic activities, which could further suppress HO_2 uptake. Lakey *et al.* found that organics suppress HO_2 uptake onto aerosols even containing TMIs,[35] and possibly the marine organisms drive discrepancies on HO_2 uptake onto seawater. The pH of the sample from Izu was buffered to 8.3, although this pH was slightly higher than that of the Hachijojima sample, given that a larger pH facilitates HO_2 uptake. This is inconsistent with the γ values obtained for the two seawater samples. Therefore, the variations of the γ values of the seawater samples should be determined based on aerosol physical chemical properties. Given the intrinsic complex composition of seawater, further investigations on the underlying uptake mechanism, which may be associated with several uncertainties related to HO_2 uptake by seawater spray, are required.

Table 3 lists the uptake coefficients of all the deliquesced aerosols detected in the present study. Basically, all the experiments were conducted under conditions with RH above 80%, higher than the deliquescence point of $(NH_4)_2SO_4$ at 298 K. NaCl aerosols have a lower deliquescence point at room temperature (75%). Thus, all the aerosols generated from the atomizer in our experiments were in the aqueous phase and were conditioned to a relatively stable RH. As indicated by the reference column in Table 3, a good agreement was observed between this study and previous studies regarding the uptake coefficients obtained. However, we expected the results to vary due to different experimental conditions, *e.g.*, TMI concentration, initial HO_2 concentration, and RH. As shown by the brown arrow with uncertainty in Fig. 4, which explicitly shows HO_2 uptake by $(NH_4)_2SO_4$, the discrepancy could be sufficiently explained taking into account the theoretic calculation of different initial HO_2 concentrations. The theoretic line in Fig. 4 was based on the conditions: pH = 4.0 (black line; pH from the current study) or 5.2 (blue line; pH from the IUPAC report[22]), r_p = 85 nm, and α = 0.7. In the comparison of the result corresponding to pH = 4 and pH = 5.2 at HO_2 concentrations below 10^9 molecules cm^{-3}, no obvious differences in the γ values were observed. Furthermore, only the results simulated at pH = 5.2 were consistent with those reported by Thornton and Abbatt who buffered the aerosol to a pH of 5.1.[36] Considering that they used a first-order analysis procedure with a high level of HO_2 radicals, the corresponding results should contain uncertainties. Details regarding the effect of pH on HO_2 loss are discussed in Section 3.3. Note that the ambient concentration of HO_2 was

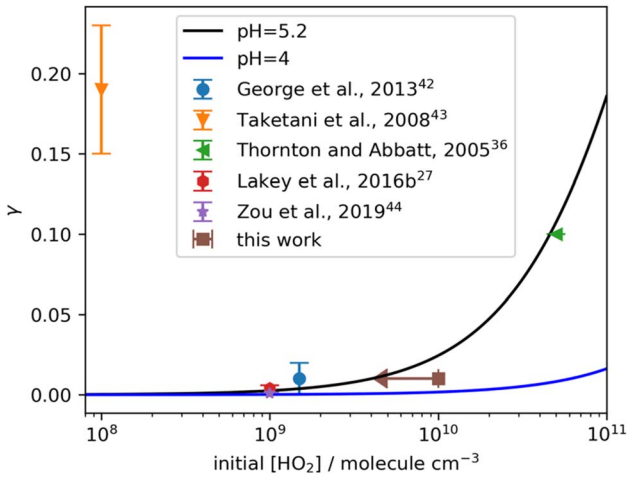

Fig. 4 Comparison of uptake coefficients onto $(NH_4)_2SO_4$ with respect to HO_2 concentration obtained in various studies and this work. The fitting lines are from the theoretical result calculated with r_p = 85 nm, α = 0.7, and pH = 5.2 (in black, pH from the IUPAC report) and 4 (in blue, pH from this work), respectively. The result from Thornton and Abbatt, 2005 (ref. 36) was conducted using $(NH_4)_2SO_4$ buffered to pH 5.1.

below 10^9 molecules cm^{-3},[37] and heterogeneous HO_2 loss onto pure $(NH_4)_2SO_4$ aerosols is limited regardless of the aerosol pH. The good agreement between our result and the theoretic calculation also supports the validity of our instrumental system.

3.3 Evaluation and comparison of the impacts of TMIs

3.3.1 TMI concentration and Henry's law constant. TMIs, such as Cu(II) and Fe(II), act as catalysts and convert HO_2 into O_2 and H_2O_2. In the aqueous phase, HO_2 usually exists in equilibrium with O_2^- and the equilibrium position is pH dependent. Hence, the kinetic reactions may include $HO_2/O_2^-/H_2O_2$. Furthermore, O_2^- reacts with TMIs, resulting in the aerosol phase attaining a larger pH with the generation of OH^-. These processes occur rapidly in the aqueous phase; the corresponding second-order rate constants at room temperature are listed in Table 4. The estimated k_{TMI} with Cu(II) in the bulk phase was expected to be at least one order of magnitude lower than the rate constants observed under aqueous solutions, as suggested in an IUPAC report that aerosols are characterized by a stronger ionic strength effect.[22] Essentially, ionic strength is a measure of the ionic concentration and the charge number of the ions. In most cases, ions do not fully dissociate owing to salting out or ion pairing with ions of charge ≥2.[38] Therefore, the activity of the ions was used instead of their concentration to evaluate the ionic strength. Eqn (16) shows the activity of the species C (A_c) as a function of its concentration multiplied by its activity coefficient (φ_c). In this study, the concentration of TMIs in the aerosol phase was simulated using the thermodynamical E-AIM model, which takes into account the activity coefficients of major ions. The activity coefficient also influences the value of the equilibrium constant, K_{eq}; however, the analysis was not adjusted for this in this study. As a result, the [Fe(II)] to [Cu(II)] ratio was 0.6–

Open Access Article. Published on 24 August 2023. Downloaded on 5/25/2026 11:43:11 AM.
This article is licensed under a Creative Commons Attribution-NonCommercial 3.0 Unported Licence.

Table 4 Previously reported rate constants of transition metal ions (TMIs) with HO_2 in the aqueous phase and the kinetic second-order rate coefficients of TMIs with HO_2/O_2^- in the aerosol phase determined in the present study

	Rate constant k_{TMIs} (M^{-1} s^{-1})				
	Cu^{2+}/Cu^{+}	References	Fe^{3+}/Fe^{2+}	References	$k_{Cu^{2+}}/k_{Fe^{2+}}$
$HO_2 + M^{(n+1)+} \rightarrow M^{n+} + H^+ + O_2$	1.0×10^8	Jacob (2000)[6]	3.1×10^5	Rush and Bielski (1985)[46]	323
$HO_2 + M^{n+}(+H^+) \rightarrow M^{(n+1)+} + H_2O_2$	1.5×10^9	Jacob (2000)[6]	2.1×10^6	Jayson *et al.* (1969)[47]	714
$O_2^- + M^{(n+1)+} \rightarrow M^+ + O_2$	8.0×10^9	Piechowski *et al.* (1993)[48]	5.0×10^7	Kang *et al.* (2002)[49]	160
$O_2^- + M^{n+}(+2H_2O) \rightarrow M^{(n+1)+} + H_2O_2 + 2OH^-$	9.4×10^9	Piechowski *et al.* (1993)[48]	1.0×10^7	Rush and Bielski (1985)[46]	940
Reactions in the aerosol phase	1.5×10^7	This work	1.3×10^5	This work	115

1.0 as indicated in Table A3.† Note that Cu(II) and Fe(II) have the same charge number and thus, should have the same ionic strength in the aerosol phase.[30]

$$A_c = [C]\varphi_c \quad (16)$$

In addition, Henry's law constant for HO_2 radicals is affected by the salting-out effect;[38] thus, it is necessary to consider correcting the activity coefficient of HO_2 taking this factor into account. For neutral molecules, such as HO_2 and under high ionic strength conditions, we set the corrected Henry's law constant, $H_c \approx H$, in the calculation. However, uncertainty with respect to H_c could bring about errors in the determination of the kinetic rate constants. Such uncertainties regarding the activity of ions or molecules should be considered in future studies.

3.3.2 pH of aerosols. An increase in the HO_2 uptake coefficient with an increase in pH was expected owing to the accelerated dissociation of HO_2 into O_2^- considering that HO_2 is a weak acid ($pK_a = 4.7$).[10] Therefore, aerosol pH has a significant effect on the kinetics in the bulk phase. The liquid solution of $(NH_4)_2SO_4$ inorganics with and without TMIs had pH 5.5–6. We used the thermodynamic model to extrapolate the aerosol pH based on the E-AIM model, which considers the activity coefficient of H^+ and the evaporation rate of water vapor. Furthermore, we evaluated the effects of the dissolved TMIs in the equilibrium state assuming the same ratio of ions as in the liquid phase to calculate the corresponding aerosol pH (Table 5).

3.3.3 Kinetic rate constant. Based on TMI concentration and aerosol pH, we could assess the kinetic rate constant (k_{TMI}) using the resistance model. Fig. 5 shows the measured HO_2 uptake coefficient onto $(NH_4)_2SO_4$ as a function of the Cu(II) concentration in the aerosol phase. Our experimental results supported the idea that the uptake coefficient increased only when the Cu(II) concentration was greater than 10^{-4} M, which is consistent with the results reported by Lakey *et al.*[35] The theoretical line with a modelled pH of 4.0 showed good agreement with our experimental dots, from which a k_{TMI} value of 1.5×10^7 M^{-1} s^{-1} was obtained. A similar rate constant (1.2×10^7 M^{-1} s^{-1}) was observed in an aqueous solution with a pH of 4,[39] and the value increased with the co-existence of Cu(II).[20] In the evaluation of kinetics with the aerosol phase, IUPAC used the following aerosol conditions: pH = 5.2, $r_p = 100$ nm, and $\alpha = 0.3$ for the calculation based on a fitting of the experimental result

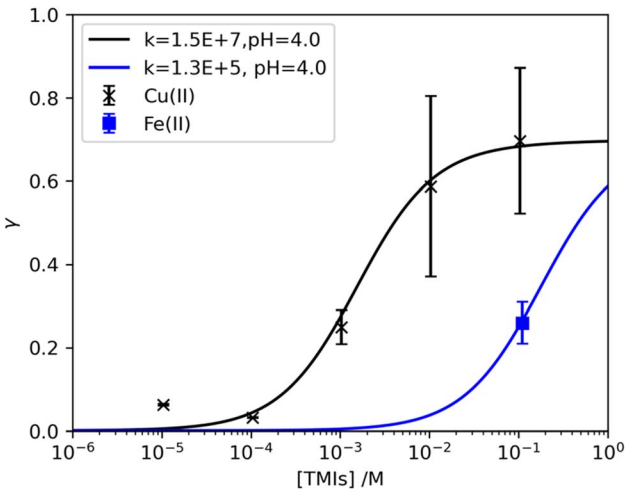

Fig. 5 HO_2 uptake coefficient as a function of the estimated [TMIs] in the aerosol phase. The solid lines represent the resistance model estimated with $r_p = 85$ nm, $[HO_2] = 1 \times 10^{10}$ molecules cm^{-3}, and $\alpha = 0.7$.

Table 5 Aerosol pH estimated from the thermodynamic model and with the participation of TMIs

	pH in the aerosol phase, E-AIM	pH with dissolved Cu(II) ions in the aerosol phase[a]	pH with dissolved Fe(II) ions in the aerosol phase[a]
NaCl	7.3	5.8	7.0
$(NH_4)_2SO_4$	4.0	4.0	4.0
Na_2SO_4	7.3	6.0	7.1

[a] Calculated from aqion 8.1.5 (https://www.aqion.de/). TMIs: transition metal ions.

© 2023 The Author(s). Published by the Royal Society of Chemistry

Open Access Article. Published on 24 August 2023. Downloaded on 5/25/2026 11:43:11 AM.
This article is licensed under a Creative Commons Attribution-NonCommercial 3.0 Unported Licence.

from Lakey *et al.*,[35] and they obtained a k_{TMI} value of 5×10^5 M^{-1} s^{-1}.[22] When we factored in the same k_{TMI} from the theoretical simulation, it was found that the aerosol pH has to be as high as 6.2 to fit the experimental dots; and the value obtained could only explain the results well corresponding to the high Cu(II) molarity region. Fig. A3† shows a comparison of k_{TMI} as a function of the uptake coefficient of HO_2 under different pH scenarios. The kinetic rate constant of HO_2 with Cu(II)-doped $(NH_4)_2SO_4$ in the aerosol phase was 1.5×10^7 M^{-1} s^{-1}, and this value unveiled uncertainties regarding aerosol pH, the participation of TMIs and HO_2, and side-reactions that also occurred in the bulk phase. Similarly, the recommended k_{TMI} value for Fe(II)-doped $(NH_4)_2SO_4$ based on our results is listed in Table 4, which equals 1.3×10^5 M^{-1} s^{-1}. This value was evaluated using a similar method to that from doped Cu(II) ions but not from Fe(II) dependence experimental results. Instead, we used the uptake coefficient with Fe(II) as 0.11 M, as shown in the blue square in Fig. 5. The ratio of the k_{TMI} values corresponding to the doping of Cu(II) to Fe(II) in the aerosol phase was quite close to that observed for the aqueous phase when considered step by step as shown in Table 4. As a result, the second-order rate constant of HO_2 loss in the presence of Cu(II) was found to be two orders of magnitude higher than that obtained in the presence of Fe(II). We only reported the kinetic rate constants obtained for $(NH_4)_2SO_4$ aerosols. The other aerosols were not analyzed owing to the uncertainty in aerosol pH with TMI participation (see Table 5) and the lack of TMI-dependence experimental data.

4 Conclusions and atmospheric implications

In this study, CC/LP-LIF was used to determine the uptake coefficient of HO_2 onto aqueous inorganic aerosols under humid conditions. Additionally, heterogeneous HO_2 loss onto diluted seawater samples collected from two sites was investigated, disclosing significant variations attributed to chemical properties, such as salinity or the co-existence of ions. Furthermore, the investigation of the effects of different TMIs on the uptake process revealed that Cu(II) accelerated the process two orders of magnitude faster than Fe(II). Even though Fe(II) was found to catalyze the uptake process at a slower rate relative to Cu(II), Fe is more ubiquitous than Cu in the ambient environment, based on an offline metallic element analysis of particulate matter, regardless of the sampling season and particle diameter.[40] Furthermore, the Cu/Fe ratio in the coarse particles was found to be less than 0.06 according to an investigation conducted close to a railway line.[41] Thus, both Cu(II) and Fe(II) should be considered given their roles in the heterogeneous processes in ambient environments. However, the experimental results regarding Cu–Fe redox coupling are not available in the current paper. Fe(II) in the aqueous or aerosol phase may be oxidized to Fe(III) in the presence of molecular oxygen or HO_2, which should be more stable than sole Fe(II). However, the relative low concentration of Fe(II) in the solution, the absence of the Fe-binding ligand, fast time resolution, and the experimental procedure sustain Fe(II) as the major redox state. The effect of Fe(III) can be ignorable (within uncertainty) regarding the value of the uptake coefficient under our laboratory conditions. Note that the co-existence of Fe(II) and minor Fe(III) may bring about uncertainties to unconsidered side-reactions, which is beyond the scope of the current study. This study provides a comparison of the kinetic rate coefficients of HO_2 loss onto $(NH_4)_2SO_4$ with different TMIs and revealed that the bulk phase reactions occurred at a lower rate than that observed for the aqueous phase (see Table 4). This could possibly be attributed to the stronger ionic strength effects in the bulk phase. The ion type was also identified as a key factor affecting the kinetic process; this requires further investigation.

Uncertainties existed in the estimation of k_{TMI} given that aerosols are associated with several uncertain parameters. First, aerosol pH is critical for determining the kinetic parameters of bulk reactions; however, the effect of pH in this regard still remains unclear. This was confirmed by Fig. A3,† which shows that the theoretical value of k_{TMI} varied approximately 30-fold when the pH increased from 4 to 6. Additionally, our estimation of the kinetic second-order rate coefficient in the presence of Cu(II)-doped $(NH_4)_2SO_4$ was the same as that recommended by Song *et al.*[10] Note that in addition to pH, the value obtained based on our results is associated with other uncertainties, including kinetic parameter assumptions and unconsidered side-reactions.

Overall, in this study, we established the detection of HO_2 onto deliquesced inorganic aerosols with different chemical compositions using the CC/LP-LIF technique. These results clarify poorly understood multiphase reactions and can aid in the optimization of model-based simulations of oxidant generation in ambient environments, especially when considering complex TMI-containing aerosols such as sea spray in marine regions. Our results also suggest that model studies need to consider different HO_2 uptake coefficients onto diverse ambient aerosols to bridge the gap with observation results. In future, it would be necessary to investigate the impact of aerosol pH, effective ion concentrations in the aerosol phase, Cu(II) or Fe(II) concentration dependence, and the water content of aerosols (phase-change effects). It would also be necessary to investigate ambient complex aerosols and detect RO_2 uptake. Additionally, the results can be combined with a 3-D model for multiphase investigations so as to ensure a better understanding of the associated heterogeneous reactions, ozone formation, and the HO_x radical budget spatiotemporally.

Data availability

Data will be made available upon request.

Author contributions

JL: data curation, formal analysis, investigation, visualization, writing-original draft preparation, and writing-review and editing; YS: project administration, supervision, validation, and writing-review and editing; KS: funding acquisition, resources, supervision, and writing-review and editing; YM: formal

Open Access Article. Published on 24 August 2023. Downloaded on 5/25/2026 11:43:11 AM. This article is licensed under a Creative Commons Attribution-NonCommercial 3.0 Unported Licence.

analysis, software, and writing-review and editing; and YK: conceptualization, funding acquisition, supervision, and writing-review and editing.

Conflicts of interest

There is no conflict to declare.

Acknowledgements

We thank Dr Hiroshi Koshikawa (National Institute for Environmental Studies) for providing the Hachijojima seawater samples. We gratefully acknowledge discussions with Dr Kentaro Murano. This study was supported by the Japan Society for the Promotion of Science (JSPS) KAKENHI (grant numbers. JP16H06304, JP19H04255, JP21H04926, and JP23K17029), the Environmental Research and Technology Development Fund (JPMEERF20215002) of the Environmental Restoration and Conservation Agency of Japan and the FY2021 National Institute for Environmental Studies Research Funding (Type A).

References

1 D. E. Heard and M. J. Pilling, Measurement of OH and HO_2 in the troposphere, *Chem. Rev.*, 2003, **103**, 5163–5198.
2 A. Khaled, M. Zhang and B. Ervens, The number fraction of iron-containing particles affects OH, HO_2 and H_2O_2 budgets in the atmospheric aqueous phase, *Atmos. Chem. Phys.*, 2022, **22**, 1989–2009.
3 X. Ren, W. H. Brune, A. Oliger, A. R. Metcalf, J. B. Simpas, T. Shirley, J. J. Schwab, C. Bai, U. Roychowdhury, Y. Li, C. Cai, K. L. Demerjian, Y. He, X. Zhou, H. Gao and J. Hou, OH, HO_2, and OH reactivity during the PMTACS–NY Whiteface Mountain 2002 campaign: Observations and model comparison, *J. Geophys. Res.: Atmos.*, 2006, **111**, 3639–3651.
4 C. E. Kolb, R. A. Cox, J. P. D. Abbatt, M. Ammann, E. J. Davis, D. J. Donaldson, B. C. Garrett, C. George, P. T. Griffiths, D. R. Hanson, M. Kulmala, G. McFiggans, U. Pöschl, I. Riipinen, M. J. Rossi, Y. Rudich, P. E. Wagner, P. M. Winkler, D. R. Worsnop and C. D. O'Dowd, An overview of current issues in the uptake of atmospheric trace gases by aerosols and clouds, *Atmos. Chem. Phys.*, 2010, **10**, 10561–10605.
5 L. K. Whalley, K. L. Furneaux, A. Goddard, J. D. Lee, A. Mahajan, H. Oetjen, K. A. Read, N. Kaaden, L. J. Carpenter, A. C. Lewis, J. M. C. Plane, E. S. Saltzman, A. Wiedensohler and D. E. Heard, The chemistry of OH and HO_2 radicals in the boundary layer over the tropical Atlantic Ocean, *Atmos. Chem. Phys.*, 2010, **10**, 1555–1576.
6 D. J. Jacob, Heterogeneous chemistry and tropospheric ozone, *Atmos. Environ.*, 2000, **34**, 2131–2159.
7 P. T. M. Ha, R. Matsuda, Y. Kanaya, F. Taketani and K. Sudo, Effects of heterogeneous reactions on tropospheric chemistry: A global simulation with the chemistry-climate model CHASER V4.0, *Geosci. Model Dev.*, 2021, **14**, 3813–3841.
8 P. D. Ivatt, M. J. Evans and A. C. Lewis, Suppression of surface ozone by an aerosol-inhibited photochemical ozone regime, *Nat. Geosci.*, 2022, **15**, 536–540.
9 K. Li, D. J. Jacob, H. Liao, J. Zhu, V. Shah, L. Shen, K. H. Bates, Q. Zhang and S. Zhai, A two-pollutant strategy for improving ozone and particulate air quality in China, *Nat. Geosci.*, 2019, **12**, 906–910.
10 H. Song, X. Chen, K. Lu, Q. Zou, Z. Tan, H. Fuchs, A. Wiedensohler, D. R. Moon, D. E. Heard, M. T. Baeza-Romero, M. Zheng, A. Wahner, A. Kiendler-Scharr and Y. Zhang, Influence of aerosol copper on HO_2 uptake: A novel parameterized equation, *Atmos. Chem. Phys.*, 2020, **20**, 15835–15850.
11 J. T. Bates, T. Fang, V. Verma, L. Zeng, R. J. Weber, P. E. Tolbert, J. Y. Abrams, S. E. Sarnat, M. Klein, J. A. Mulholland and A. G. Russell, Review of Acellular Assays of Ambient Particulate Matter Oxidative Potential: Methods and Relationships with Composition, Sources, and Health Effects, *Environ. Sci. Technol.*, 2019, **53**, 4003–4019.
12 J. P. S. Wong, J. P. S. Wong, Y. Yang, T. Fang, J. A. Mulholland, A. G. Russell, S. Ebelt, A. Nenes, A. Nenes, A. Nenes and R. J. Weber, Fine Particle Iron in Soils and Road Dust Is Modulated by Coal-Fired Power Plant Sulfur, *Environ. Sci. Technol.*, 2020, **54**, 7088–7096.
13 L. Deguillaume, M. Leriche, K. Desboeufs, G. Mailhot, C. George and N. Chaumerliac, Transition metals in atmospheric liquid phases: Sources, reactivity, and sensitive parameters, *Chem. Rev.*, 2005, **105**, 3388–3431.
14 W. H. Schroeder, M. Dobson, D. M. Kane and N. D. Johnson, *J. Air Pollut. Control Assoc.*, 1987, **37**, 1267–1285.
15 M. Mozurkewich, P. H. McMurry, A. Gupta and J. G. Calvert, Mass accommodation coefficient for HO_2 radicals on aqueous particles, *J. Geophys. Res.*, 1987, **92**, 4163.
16 Y. Sadanaga, A. Yoshino, K. Watanabe, A. Yoshioka, Y. Wakazono, Y. Kanaya and Y. Kajii, Development of a measurement system of OH reactivity in the atmosphere by using a laser-induced pump and probe technique, *Rev. Sci. Instrum.*, 2004, **75**, 2648–2655.
17 K. Miyazaki, Y. Nakashima, C. Schoemaecker, C. Fittschen and Y. Kajii, Note: A laser-flash photolysis and laser-induced fluorescence detection technique for measuring total HO_2 reactivity in ambient air, *Rev. Sci. Instrum.*, 2013, **84**, 10–13.
18 M. J. Tang, M. Shiraiwa, U. Pöschl, R. A. Cox and M. Kalberer, Compilation and evaluation of gas phase diffusion coefficients of reactive trace gases in the atmosphere: Volume 2. Diffusivities of organic compounds, pressure-normalised mean free paths, and average Knudsen numbers for gas uptake calculations, *Atmos. Chem. Phys.*, 2015, **15**, 5585–5598.
19 J. A. Thornton, L. Jaeglé and V. F. McNeill, Assessing known pathways for HO_2 loss in aqueous atmospheric aerosols: Regional and global impacts on tropospheric oxidants, *J. Geophys. Res.: Atmos.*, 2008, **118**(D5), D05303.
20 B. H. J. Bielski, D. E. Cabelli, R. L. Arudi and A. B. Ross, Reactivity of HO_2/O_2^- Radicals in Aqueous Solution, *J. Phys. Chem. Ref. Data*, 1985, **14**, 1041–1100.

© 2023 The Author(s). Published by the Royal Society of Chemistry

Open Access Article. Published on 24 August 2023. Downloaded on 5/25/2026 11:43:11 AM.
This article is licensed under a Creative Commons Attribution-NonCommercial 3.0 Unported Licence.

21 D. R. Hanson and A. R. Ravishankara, Reactive Uptake of $ClONO_2$ onto Sulfuric Acid Due to Reaction with HCl and H_2O, *J. Phys. Chem.*, 1994, **98**, 5728–5735.
22 M. Ammann, R. A. Cox, J. N. Crowley, M. E. Jenkin, A. Mellouki, M. J. Rossi, J. Troe and T. J. Wallington, *IUPAC Task Group on Atmospheric Chemical Kinetic Data Evaluation*, 2013.
23 S. L. Clegg, P. Brimblecombe and A. S. Wexler, Thermodynamic model of the system H^+–NH_4^+–Na^+–SO_4^{2-}–NO_3^-–Cl^-–H_2O at 298.15 K, *J. Phys. Chem. A*, 1998, **102**, 2155–2171.
24 Simon Clegg, E-AIM Home Page, **http://www.aim.env.uea.ac.uk/aim/aim.php**, accessed 24 October 2022.
25 A. Nenes and S. N. Pandis, ISORROPIA: A New Thermodynamic Equilibrium Model for Multiphase Multicomponent Inorganic Aerosols, *Aquat. Geochem.*, 1998, **4**, 123–152.
26 C. Fountoukis and A. Nenes, Atmospheric Chemistry and Physics ISORROPIA II: a computationally efficient thermodynamic equilibrium model for K^+–Ca^{2+}–Mg^{2+}–NH_4^+–Na^+–SO_4^{2-}–NO_3^-–Cl^-–H_2O aerosols, *Atmos. Chem. Phys.*, 2007, **7**, 4639–4659.
27 P. S. J. Lakey, T. Berkemeier, M. Krapf, J. Dommen, S. S. Steimer, L. K. Whalley, T. Ingham, M. T. Baeza-Romero, U. Pöschl, M. Shiraiwa, M. Ammann and D. E. Heard, The effect of viscosity and diffusion on the HO_2 uptake by sucrose and secondary organic aerosol particles, *Atmos. Chem. Phys.*, 2016, **16**, 13035–13047.
28 I. J. George and J. P. D. Abbatt, Heterogeneous oxidation of atmospheric aerosol particles by gas-phase radicals, *Nat. Chem.*, 2010, **2**, 713–722.
29 J. Wei, T. Fang, P. S. J. Lakey and M. Shiraiwa, Iron-Facilitated Organic Radical Formation from Secondary Organic Aerosols in Surrogate Lung Fluid, *Environ. Sci. Technol.*, 2022, **56**, 7234–7243.
30 J. Mao, S. Fan, D. J. Jacob and K. R. Travis, Radical loss in the atmosphere from Cu-Fe redox coupling in aerosols, *Atmos. Chem. Phys.*, 2013, **13**, 509–519.
31 J. Mao, S. Fan and L. W. Horowitz, Soluble Fe in Aerosols Sustained by Gaseous HO_2 Uptake, *Environ. Sci. Technol. Lett.*, 2017, **4**, 98–104.
32 P. S. J. Lakey, I. J. George, L. K. Whalley, M. T. Baeza-Romero and D. E. Heard, Measurements of the HO_2 uptake coefficients onto single component organic aerosols, *Environ. Sci. Technol.*, 2015, **49**, 4878–4885.
33 F. Taketani, Y. Kanaya and H. Akimoto, Heterogeneous loss of HO_2 by KCl, synthetic sea salt, and natural seawater aerosol particles, *Atmos. Environ.*, 2009, **43**, 1660–1665.
34 F. J. Millero, R. Feistel, D. G. Wright and T. J. McDougall, The composition of Standard Seawater and the definition of the Reference-Composition Salinity Scale, *Deep-Sea Res. Part I Oceanogr. Res. Pap.*, 2008, **55**, 50–72.
35 P. S. J. Lakey, I. J. George, M. T. Baeza-Romero, L. K. Whalley and D. E. Heard, Organics Substantially Reduce HO_2 Uptake onto Aerosols Containing Transition Metal ions, *J. Phys. Chem. A*, 2016, **120**, 1421–1430.
36 J. Thornton and J. P. D. Abbatt, Measurements of HO_2 uptake to aqueous aerosol: Mass accommodation coefficients and net reactive loss, *J. Geophys. Res. Atmos.*, 2005, **110**, 1–12.
37 F. Holland, A. Hofzumahaus, J. Schäfer, A. Kraus and H. W. Pätz, Measurements of OH and HO_2 radical concentrations and photolysis frequencies during BERLIOZ, *J. Geophys. Res.: Atmos.*, 2003, **108**(D4), 8246.
38 D. C. Harris, *Quantitative Chemical Analysis*, Craig Bleyer, California, 7th edn, 2007, vol. 1, pp. 140–146.
39 B. H. J. Bielski and A. O. Allen, Mechanism of the disproportionation of superoxide radicals, *J. Phys. Chem.*, 1977, **81**, 1048–1050.
40 N. T. Hieu and B. K. Lee, Characteristics of particulate matter and metals in the ambient air from a residential area in the largest industrial city in Korea, *Atmos. Res.*, 2010, **98**, 526–537.
41 N. Bukowiecki, R. Gehrig, M. Hill, P. Lienemann, C. N. Zwicky, B. Buchmann, E. Weingartner and U. Baltensperger, Iron, manganese and copper emitted by cargo and passenger trains in Zürich (Switzerland): Size-segregated mass concentrations in ambient air, *Atmos. Environ.*, 2007, **41**, 878–889.
42 I. J. George, P. S. J. Matthews, L. K. Whalley, B. Brooks, A. Goddard, M. T. Baeza-Romero and D. E. Heard, Measurements of uptake coefficients for heterogeneous loss of HO_2 onto submicron inorganic salt aerosols, *Phys. Chem. Chem. Phys.*, 2013, **15**, 12829–12845.
43 F. Taketani, Y. Kanaya and H. Akimoto, Kinetics of heterogeneous reactions of HO_2 radical at ambient concentration levels with $(NH_4)_2SO_4$ and NaCl aerosol particles, *J. Phys. Chem. A*, 2008, **112**, 2370–2377.
44 Q. Zou, H. Song, M. Tang and K. Lu, Measurements of HO_2 uptake coefficient on aqueous $(NH_4)_2SO_4$ aerosol using aerosol flow tube with LIF system, *Chin. Chem. Lett.*, 2019, **30**, 2236–2240.
45 P. Sylvie and J. Matthews, PhD thesis, The University of Leeds, 2014.
46 J. D. Rush and B. H. J. Bielski, Pulse Radlolytic Studies of the Reactions of HO_2/O_2^- with Fe(II)/Fe(III) Ions. The Reactivity of HO_2/O_2^- with Ferric Ions and Its Implication on the Occurrence of the Haber-Weiss Reaction, *J. Phys. Chem.*, 1985, **89**, 5062–5066.
47 G. G. Jayson, J. P. Keene, D. A. Stirling and A. J. Swallow, Pulse-Radiolysis Study of Some Unstable Complexes of Iron, *Trans. Faraday Soc.*, 1969, **65**, 2453–2464.
48 M. Von Piechowski, T. Nauser, J. Hoignè and R. E. Bühler, O_2^- Decay Catalyzed by Cu^{2+} and Cu^+ Ions in Aqueous Solutions: A Pulse Radiolysis Study for Atmospheric Chemistry, *Berichte der Bunsengesellschaft für physikalische Chemie*, 1993, **97**, 762–771.
49 N. Kang, D. S. Lee and J. Yoon, Kinetic modeling of Fenton oxidation of phenol and monochlorophenols, *Chemosphere*, 2002, **47**, 915–924.